Acoust. Sci. & Tech. **30**, 4 (2009)

PAPER

Propagation of fast and slow waves in cancellous bone: Comparative study of simulation and experiment

Yoshiki Nagatani[1,*], Katsunori Mizuno[2], Takashi Saeki[2], Mami Matsukawa[3,†], Takefumi Sakaguchi[4] and Hiroshi Hosoi[4]

[1]*Department of Electronic Engineering, Kobe City College of Technology*
[2]*Graduate School of Engineering, Doshisha University*
[3]*Faculty of Life and Medical Sciences, Graduate School of Engineering, Doshisha University*
[4]*Department of Otorhinolaryngology–Head and Neck Surgery, Faculty of Medicine, Nara Medical University*

(*Received 31 July 2008, Accepted for publication 23 January 2009*)

Abstract: Comparative study of longitudinal wave propagation in cancellous bone was performed. We simulated wave propagation with the finite-difference time-domain (FDTD) method using a three-dimensional X-ray computer tomography (CT) model of an actual cancellous bone. We also experimentally measured the waves that propagated in an identical specimen under similar conditions. The speeds of fast waves and the amplitudes of fast and slow waves at small ROIs (region of interest) in the specimen were examined. We found good correlations in fast wave speed and wave amplitudes between simulated and measured data. The peak amplitude ratio of simulated two waves was also similar with the experimental results. These results show the importance of FDTD simulation to understand the wave propagation phenomena in the complicated medium.

Keywords: Cancellous bone, Fast wave, Slow wave, X-ray CT, Three-dimensional elastic FDTD method

PACS number: 43.35.+d, 43.80.+p [doi:10.1250/ast.30.257]

1. INTRODUCTION

Considering the aging of Japanese society, demand is growing for a more reliable and less onerous method of diagnosing osteoporosis. Ultrasonic diagnosis systems are considered a powerful tool, because ultrasonic waves strongly reflect the elasticity. The current *in vivo* ultrasonic diagnosis technique is the "Speed Of Sound/Broadband Ultrasound Attenuation" (SOS/BUA) method [1]; however, as a simple measurement of averaged ultrasonic wave speed and attenuation of whole bone in the wave propagation path, this method does not really reflect the precise bone structure and the amount of minerals present.

In order to improve the accuracy of ultrasonic diagnosis system, our group has proposed a new approach to evaluate bone that utilizes the separation of longitudinal waves as they pass through cancellous bone [2–4]. We have reported the separation of longitudinal waves into fast and slow waves, a phenomenon that is especially dependent upon the alignment of bone trabecula in cancellous bone [5–7]. It is hoped that this interesting phenomenon will become a powerful tool in the diagnosis of osteoporosis because the wave propagation behavior apparently depends on the bone structure. However, the details of wave propagation in cancellous bone have not yet been examined, because of the structural complexity and inhomogeneity.

Several theoretical approaches have been taken to elucidate the phenomenon of wave propagation in porous material. In Biot's theory [8], or the multi-layer model [9], the porous structure is described according to several parameters in an effort to predict the generation of fast and slow waves in cancellous bone. Hosokawa has reported the separation of waves by means of a numerical solution using Biot's theory with the finite-difference method [10]; however, difficulties in bone analysis remain because of the limited applicability of Biot's theory to cancellous bone [11,12], which exhibits significant anisotropy and inhomogeneity.

The difficulties of analytic evaluation have led to the direct approach of attempting to solve the wave equation. If an exact simulation of wave propagation were to succeed,

*e-mail: nagatani@kobe-kosen.ac.jp
†e-mail: mmatsuka@mail.doshisha.ac.jp

it would give us a visual image of complicated wave propagation in the bone. This would be helpful for constructing a novel and optimum *in vivo* ultrasonic measurement system [13].

Using a three-dimensional (3-D) synchrotron micro-tomograph of actual trabecula, Bossy *et al.* [14] and Padilla *et al.* [15] reported the generation of fast and slow waves using finite-difference time-domain (FDTD) simulation. Haïat *et al.* [16] investigated the influence of trabecular bone microstructure and material properties on SOS/BUA parameters using numerical simulations. However, a quantitative comparison between simulation and experimental results has not been investigated. Therefore, our group sought to confirm the applicability of the elastic FDTD method to the simulation of wave propagation in cancellous bone using three-dimensional X-ray CT images [17,18] by focusing on the comparative studies between the FDTD simulation and experimental data. The tendency of the simulated results showed good agreement with experimental data; however, there were still a problem due to the lack of spatial resolution of simulation model [17]. Recent investigations of Padilla *et al.* [19] and Jenson *et al.* [20] show the similar tendency of SOS (or phase velocity) and BUA between simulated and experimental results; however, they have not examined the characteristics of two-wave phenomenon.

In this study, therefore, we simulated wave propagation in a cancellous bone with the elastic FDTD method using a more precise three-dimensional X-ray CT model of an actual cancellous bone. We also experimentally measured the waves that propagated in an identical specimen under similar conditions in order to investigate the adequacy of the simulation technique, especially focusing on the two-wave phenomenon.

2. MEASUREMENT

2.1. Experimental Setup

For this comparative study, the waves propagated through the bone were experimentally measured with PVDF transducers. The size of the bovine cancellous bone used was $20 \times 20 \times 9\ mm^3$. Figure 1 shows the photograph of the bone specimen. The specimen was obtained from the head of 36-month-old bovine femur.

During the measurements, the bone specimen was immersed in degassed water at room temperature. Before measurement, the air in the porous structure was eliminated by degassing. The geometric focal length of the star-shaped concave PVDF transmitter (custom-made by TORAY, Tokyo, Japan) was 40 mm and the radius was 10 mm. The surface of the transmitter was star-shaped in order to decrease the edge effect [21]. In water, the beam width at half maximum value of the wave amplitude was approximately 1.5 mm at the focal point [21]. The transmitted

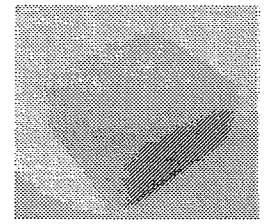

Fig. 1 Photograph of the specimen. The bone marrow inside the cancellous bone was removed.

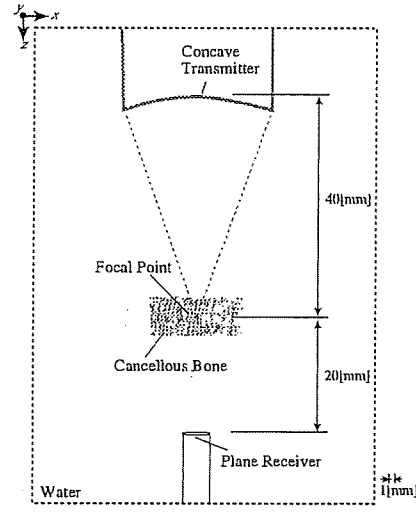

Fig. 2 Schematic representation near the specimen of the measurement system. The inside porous area and outside the specimen was filled with degassed water.

wave focused in the specimen at the mid point of the thickness. The radius of the plane PVDF receiver (home-made with PVDF film) was 2.5 mm. Figure 2 shows the measurement system. In this measurement, the bone specimen was fully immersed in water. The z-axis position of the transmitter was fixed to maintain the focal point at the mid point of the specimen thickness without consideration of refraction. The distribution of the wave properties was investigated by changing the positions of the transmitter and receiver along the x-y plane. They were moved in 1-millimeter-increments. The total number of measured points was 144.

A single sinusoidal wave at 1 MHz, 5 Vp-p from a function generator (WF1945, NF Corporation, Kanagawa, Japan) was amplified by a 20-dB power amplifier (4055, NF Corporation, Kanagawa, Japan), and applied to the transmitter. By changing the positions of the specimen along the x-y plane, we investigated the distribution of wave properties with a digital oscilloscope (TDS 524A, Tektronix Inc., Oregon, United States) with 40-dB preamplifier (5307, NF Corporation, Kanagawa, Japan).

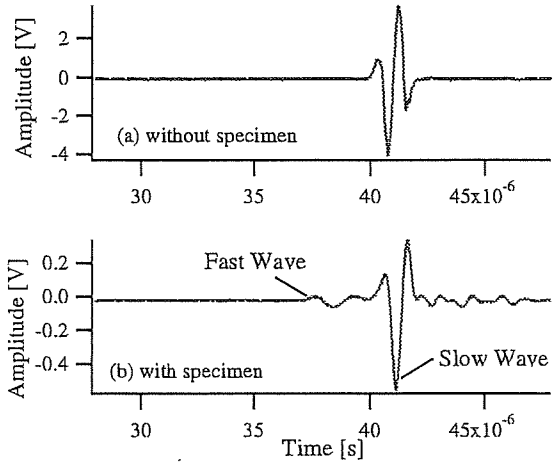

Fig. 3 Experimentally observed waveforms. Waves pass through the experimental setup, (a) without the specimen, or (b) with the specimen.

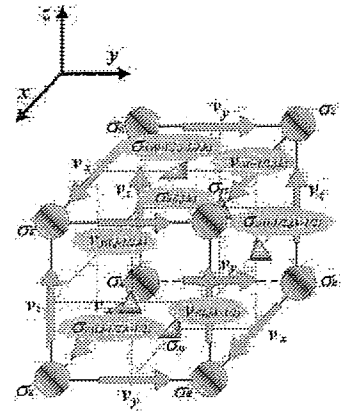

Fig. 4 The spatial configuration of the parameters of FDTD simulation.

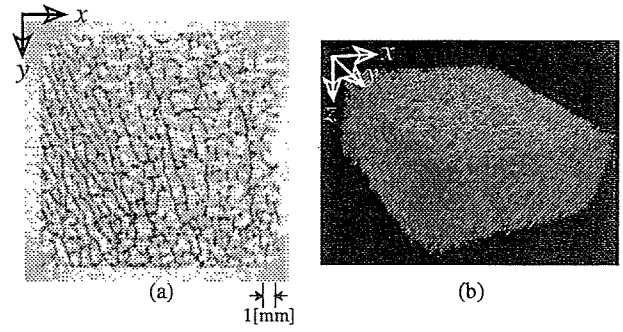

Fig. 5 A specimen of bovine cancellous bone used in the simulation and experiment. (a) One slice of the 2-D X-ray CT image before binarization. (b) 3-D reconstructed model of cancellous bone after binarization.

2.2. Experimental Results

Examples of the experimentally observed waveforms are shown in Figs. 3(a) and (b). Figure 3(a) shows the result when the transmitted wave passes only through water; Figure 3(b) shows the result when the transmitted wave is focused on the center portion of the specimen. In Fig. 3(b), the separation into fast and slow waves can be seen. Here, we adopted the first positive peak as the fast wave amplitude and the maximum amplitude of whole waveform as the slow wave amplitude.

3. SIMULATION

3.1. Elastic FDTD Method

The followings are the governing equations for the 3-dimensional elastic FDTD method [22,23] for the isotropic medium. Deputized equations related to the x direction are:

$$\frac{\partial \sigma_{xx}}{\partial t} = (\lambda + 2\mu)\frac{\partial v_x}{\partial x} + \lambda \frac{\partial v_y}{\partial y} + \lambda \frac{\partial v_z}{\partial z}, \tag{1}$$

$$\frac{\partial \sigma_{xy}}{\partial t} = \mu\left(\frac{\partial v_x}{\partial y} + \frac{\partial v_y}{\partial x}\right), \tag{2}$$

$$\frac{\partial v_x}{\partial t} = \frac{1}{\rho}\left(\frac{\partial \sigma_{xx}}{\partial x} + \frac{\partial \sigma_{xy}}{\partial y} + \frac{\partial \sigma_{zx}}{\partial z}\right), \tag{3}$$

where σ_{xx} and σ_{xy} are normal and shear stresses, v_x is particle velocity, λ and μ are Lame's coefficients, and ρ is the density of the medium. These equations are digitized using the central difference method. Figure 4 shows the configuration of the parameters of FDTD simulation. The stress and particle velocity were calculated alternately both in the spatial and time domains, which is called "the leapfrog method." Absorption layers were implemented on each end face of the model [24]. Making use of the advantage of simulation, we set the attenuation of the values of the normal and shear stresses in each calculation step of wave propagation, considering dx (spatial resolution). The attenuation for each step was determined from the experimentally observed longitudinal attenuation value of cortical bone at 1 MHz [25,26]. The attenuation used did not exhibit frequency dispersion. In this simulation, the elastic anisotropy of the solid portion was not considered.

3.2. Simulation Model

The wave propagation was simulated using the identical bone specimen that was experimentally measured in chapter 2. Figures 5(a) and (b) are X-ray micro-focus CT images (MCT-12505MF, Hitachi Medical, Tokyo, Japan). The spatial resolution of the CT images was 64.5 μm. This field was smaller than the experimental measurement area due to the memory limitaion of computer. The values of each point in the CT images were binarized in order to allow separation of the ambiguous border between the solid portions (trabecula) and liquid portions at a specific threshold. The threshold was determined as the median value of the grayscale tones of the image.

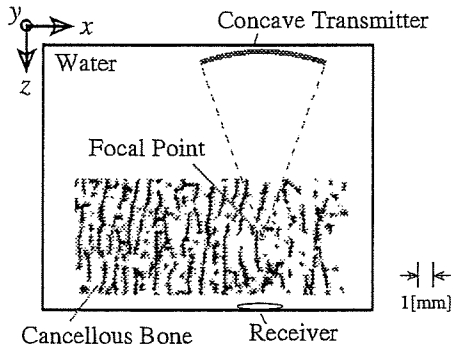

Fig. 6 The FDTD simulation model. The concave transmitter faces the specimen immersed in water. Absorption layers were implemented on each end face of the model.

The total simulation field was $23 \times 23 \times 18\,\mathrm{mm}^3$ with cube lattice of 64.5 μm. The time increment of simulation was 5 ns. As the initial particle velocity in z direction at the surface of the concave source shown in Fig. 6, the single sinusoidal wave at 1 MHz was used. The Hanning window whose length was 1 μs was applied to prevent the discontinuity of the waveform.

In this simulation, the surface of the transmitter was star-shaped in order to decrease the edge effect [21]. This comes from the actual transducer used in the experiments. The surface polygon had 16 apexes. The outer radius of the star shape was 2.5 mm and the inside radius was 1.25 mm. The geometric focal length of concave transmitter was 10 mm. Because of the lack of memory capacity of the computer, the configuration of the transmitter in this simulation was set proportional to the actual experimental system. The receiver was 1.5 mm in radius, and the results of the simulated sound pressures were obtained from the integrated values on the receiver surface, where the sound waves were not reflected nor interrupted. The transmitter and the receiver have the acoustical axis in common.

In this model, the bone specimen was fully immersed in water. The z-axis position of the transmitter was fixed to maintain the focal point at the mid point of the specimen thickness without considering the refraction. The distribution of the wave propagation was investigated by changing the positions of the transmitter and receiver in the x-y plane. They were moved in about 1-millimeter-increments. The total number of simulated points was 144.

The experimentally observed values in the bovine cortical bone were used as the wave speed and attenuation in the trabeculae part of the cancellous bone. Yamato *et al.* [27–29] reported that the speed of the longitudinal wave in cortical bone varied from 4,000 to 4,400 m/s. In this study, the simulations were performed at the longitudinal wave speed of 4,400 m/s because much higher velocities were reported in the trabeculae in the GHz range [30]. In the simulation, the speed of shear wave was the estimated value, assuming Poisson's ratio of 0.34 [2]. We adopted the experimentally observed attenuation in the cortical bone as the attenuation coefficients of longitudinal wave in trabeculae [25,26]. The attenuation coefficient of the shear wave in the solid portion was estimated as twice that of the longitudinal wave, considering the properties of polymeric materials [31]. The parameters used in this simulation are shown in Table 1. The FDTD simulation software was originally programmed by our group [32].

Table 1 Parameters used in the FDTD simulation.

Material		Water	Bone trabecula
Density [10^3 kg/m^3]		1.0	2.0
Velocity [m/s]	Longitudinal	1,500	4,400
	Shear	—	2,200
Lame's constant [GPa]	λ	2.2	20.0
	μ	—	9.4
Attenuation [neper/m]	Longitudinal	0.025	80
	Shear	—	160

3.3. Numerical Results

Figures 7 show the screenshots of the distribution of sound pressure (in liquid portion) or root-mean-square value of normal stresses (in solid portion) at the central x-y plane of the three-dimensional simulation field. Figures (a) to (c) show the results without specimen, (d) to (f) show the results with specimen. The separation of fast wave and slow wave can be seen [18].

The calculated waveforms are shown in Figs. 8(a) and (b). Figure 8(a) shows the result when the transmitted wave passes only through the water. The slight vibration at the tail of the waveform in Fig. 8(a) seems to result from the spatial resolution in simulating. Figure 8(b) shows the result when the wave is focused on the center portion of the specimen, which is in a simular condition to that of Fig. 3(b). The estimated BV/TV (bone volume/total tissue volume, or bone volume fraction) around the area of this result was 32.9%. Here, the BV/TV is the averaged value of the cuboidal area in the model of $3 \times 3 \times 9\,\mathrm{mm}^3$ around the focal point of the concave source. This cuboidal ROI (region of interest) was estimated considering the focal area of transmitted wave in experiments [7]. Here, both fast and slow waves can be seen. The fast wave is considered to propagate mainly in the solid portion of bone specimen. The amplitude of the fast wave was smaller than that of the slow wave, which has also been reported from experimental studies [2–4].

4. DISCUSSION

In these simulations and experiments, we obtained the peak amplitudes of the fast and slow waves and the speed of

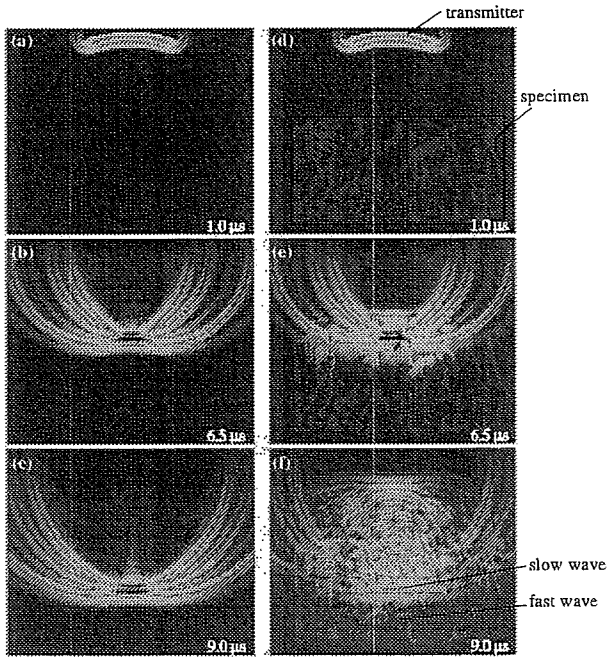

Fig. 7 Screenshots of the distribution of sound pressure in the x-z plane of the three-dimensional simulation field inluding the specimen center. Figures (a) to (c) show the results without specimen, (d) to (f) show the results with specimen.

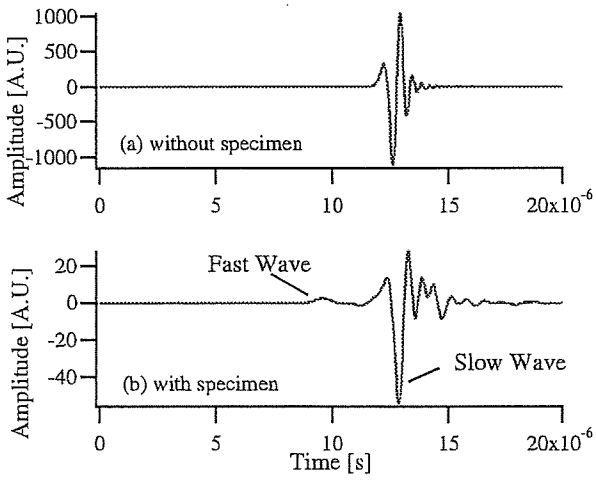

Fig. 8 Simulated waveforms. Waves pass through the simulation model, (a) without the specimen, or (b) with the specimen.

the fast wave estimated from the arrival time of the wave front. Here, we adopted the first positive peak as the fast wave amplitude and the maximum amplitude of whole waveform as the slow wave amplitude. In this study, we could not obtain the speed of slow waves because superposition with fast waves affected the wave fronts of the slow waves.

Figure 9(a) shows the relationship between BV/TV around the focal point and the speed of the fast wave. We can see correlations in both the simulated and experimental results. Both results increased in proportion to the BV/TV. This indicates that the fast wave speed depends on the amount of trabecula in the wave propagation path.

The relationships between the BV/TV and the peak amplitude of the fast and slow waves are shown in Figs. 9(b)(c). Here, all values are normalized by the peak amplitude of the wave that passed only through the water. The amplitude of the fast wave has a positive correlation to the BV/TV, while the amplitude of the slow wave has a negative correlation. The fast wave passes mainly through the solid portion (trabeculae) and the slow wave passes mainly through the liquid portion [2–4]. The increase in the BV/TV results in a minimization of liquid path or the generation of closed liquid portions surrounded by solid bone, which rapidly increases the amplitude of the fast wave and contrarily decreases that of the slow wave. These characteristics are also supported by the former experimental studies [2,3,7].

Table 2 shows the correlation coefficients of the BV/TV and each indicator of the simulated and experimental results. These data show clear correlation between simulations and experiments: The correlation coefficients of the fast wave speed, the amplitudes of the fast and slow waves between simulation and experiments were 0.58, 0.74, and 0.83 ($p < 0.01$), although we adopted the velocity and attenuation values of cortical bone, because the values in the trabeculae are unknown. There seem to be other causes for these differences in addition to the velocity and attenuation values. For example, the selection of the threshold for the modeling of CT image [16,33] and present assumption of isotropic elasticity in the trabeculae. We also should point the difference of simulation field from the measurement due to memory problem: The transmitter in the simulation was smaller than that in the actual experimental system, which results in wider beam width at the focal area because the ratios of the wavelength and the radius of the transducer are disparate. In addition, due to the limitation of simulation field, we put the smaller receiver near the specimen. We can also point out the effect of the frequency dispersion of attenuation coefficients in trabeculae, and the influence of boundary friction at the interface of the liquid and solid portions [17]. These problems should be considered in future studies.

Despite the problems, however, the simulation reveals some interesting results. Figure 9(d) shows the relationships between the BV/TV and the peak amplitude ratio between fast and slow waves. Differences at low BV/TV area in Fig. 9(c) and high BV/TV area in Fig. 9(b) disappeared. Some agreements between the simulated and experimental results becomes apparent. The amplitude ratio concerns the separation mechanism of the initial wave into the fast and slow waves; therefore, this agreement of simulation and experiment suggests the possibility of

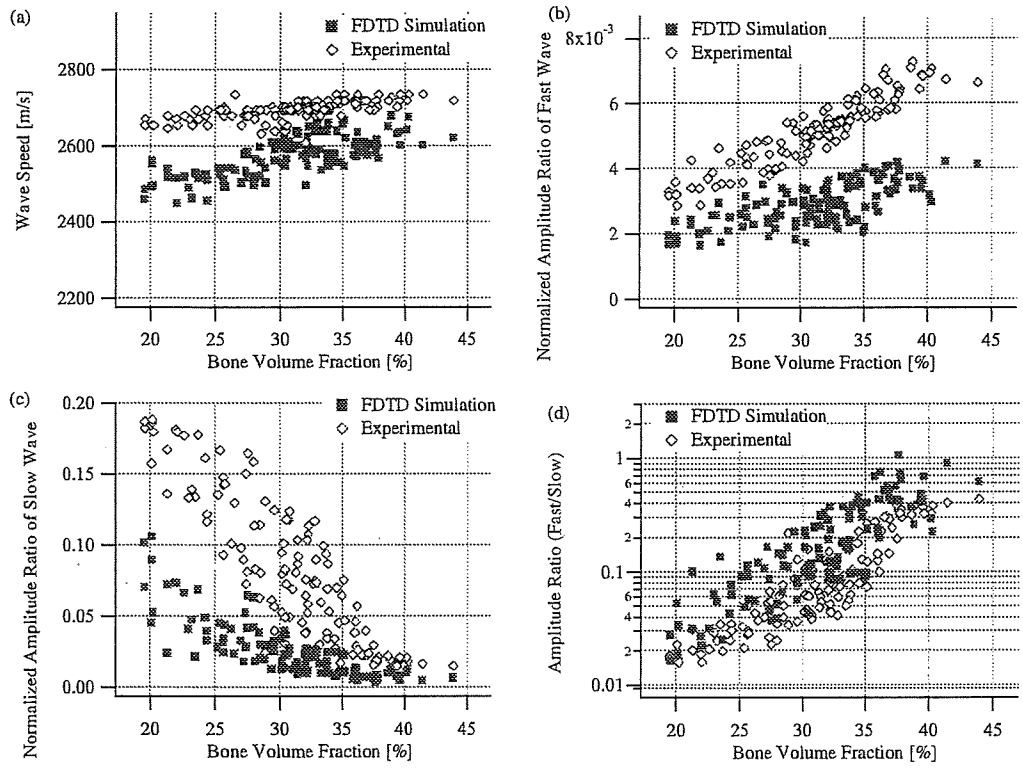

Fig. 9 Relationship between BV/TV (bone volume fraction) and (a) speed of fast wave, (b) peak amplitude of fast wave, (c) peak amplitude of slow wave, and (d) peak amplitude ratio of fast and slow waves. The longitudinal wave speed was assumed to be 4,400 m/s. All values are normalized by the peak amplitude of the wave that passed through the water only. The same unique specimen was used for both the simulation and the experiment.

Table 2 Correlation coefficients (R) of (i) BV/TV v.s. simulated results, (ii) BV/TV v.s. experimental results, and (iii) simulated results v.s. experimental results. ($p < 0.01$ in all cases).

Indicator	(i) BV/TV v.s. Simulation	(ii) BV/TV v.s. Experiment	(iii) Simulation v.s. Experiment
Wave speed	0.71	0.66	0.58
Normalized amplitude ratio of fast wave	0.69	0.93	0.74
Normalized amplitude ratio of slow wave	−0.81	−0.87	0.83

understanding the generation mechanism of wave separation by FDTD simulation using X-ray CT images. The separation phenomena of longitudinal wave into fast and slow waves seems to depends on the BV/TV.

Figures 10 show the results when the londitudinal wave speed were assumed to be 4,060 m/s, where the Poisson's ratio was 0.34. A comparison of Figs. 9 and 10 clarifies that the selection of the longitudinal wave speed in the trabeculae affects the results: a higher longitudinal wave speed results in not only the higher fast wave speed but also the smaller fast wave amplitude and larger slow wave amplitude. These results are believed to be caused by the change in the acoustic impedance of trabeculae, suggesting the importance of the initial properties used in the simulation. The comparison of Figs. 9 and 10 tell us that more special attenuation to the wave properties for simulation will give us better correlation between simulation and experiments.

5. CONCLUSION

Using a 3-D X-ray CT model of a bovine cancellous bone, the generation of fast and slow waves was confirmed by the elastic FDTD simulation. We also experimentally measured the waves propagated in an identical bone specimen under the same conditions. Comparing the results in detail, we found the similar tendency between the simulated and experimental results.

The simulated speed of fast wave, the peak amplitude of fast and slow waves, and the amplitude ratio between those two waves showed clear correlations with BV/TV. The discrepancy of values between experiments and simulation seems to come from the modeling difficulties

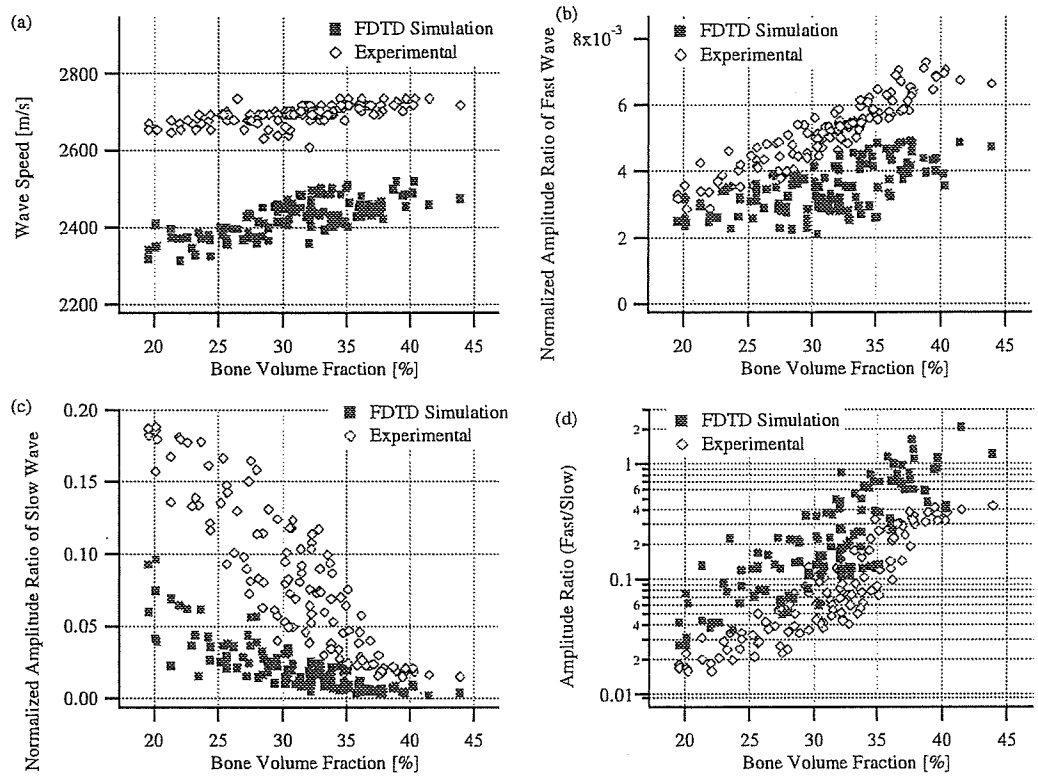

Fig. 10 Relationship between BV/TV (bone volume fraction) and (a) speed of fast wave, (b) peak amplitude of fast wave, (c) peak amplitude of slow wave, and (d) peak amplitude ratio of fast and slow waves. The longitudinal wave speed was assumed to be 4,060 m/s. The Poisson's ratio was 0.34, which is same as the condition of Fig. 9. All values are normalized by the peak amplitude of the wave that passed through the water only. The same unique specimen was used for both the simulation and the experiment.

(adopted values for wave properties, friction loss, etc.). However, the peak amplitude ratio between the fast and slow waves agreed with the experimental results. This simulation technique can help us understand wave propagation in a complicated medium and can be an effective tool for designing a new *in vivo* ultrasonic measurement system for osteoporosis.

ACKNOWLEDGMENTS

The authors like to thank Dr. Masahiko Takada at Shiga University of Medical Science for the X-ray microfocus CT.

This study was partly supported by a bilateral joint project between the Japan Society for the Promotion of Science (JSPS) and Centre National de la Recherche Scientifique (CNRS) as well as the Academic Research Frontier project of Doshisha University and the Ministry of Education, Culture, Sports, Science and Technology of Japan. In addition to the Grant-in-Aid for Young Scientists (B) (20791218) supported by JSPS, some parts of this study were also supported by the Open Competition for the Development of Innovative Technology, a project of the Ministry of Education, Culture, Sports, Science and Technology.

REFERENCES

[1] C. F. Njeh, D. Hans and T. Fuerst, *Quantitative Ultrasound: Assessment of Osteoporosis and Bone Status*, 1st ed. (Taylor & Francis, London, 1999).

[2] A. Hosokawa and T. Otani, "Ultrasonic wave propagation in bovine cancellous bone," *J. Acoust. Soc. Am.*, **101**, 558–562 (1997).

[3] A. Hosokawa, T. Otani, T. Suzaki, Y. Kubo and S. Takai, "Influences of trabecular structure on ultrasonic wave propagation in bovine cancellous bone," *Jpn. J. Appl. Phys.*, **36**, 3233–3237 (1997).

[4] T. Otani, "Quantitative estimation of bone density and bone quality using acoustic parameters of cancellous bone for fast and slow waves," *Jpn. J. Appl. Phys.*, **44**(6B), 4578–4582 (2005).

[5] I. Mano, K. Horii, S. Takai, T. Suzaki, H. Nagaoka and T. Otani, "Development of novel ultrasonic bone densitometry using acoustic parameters of cancellous bone for fast and slow waves," *Jpn. J. Appl. Phys.*, **45**(5B), 4700–4702 (2006).

[6] I. Mano, T. Yamamoto, H. Hagino, R. Teshima, M. Takada, T. Tsujimoto and T. Otani, "Ultrasonic transmission characteristics of in vitro human cancellous bone," *Jpn. J. Appl. Phys.*, **46**(7B), 4858–4861 (2007).

[7] K. Mizuno, M. Matsukawa, T. Otani, M. Takada, I. Mano and T. Tsujimoto, "Effects of structural anisotropy of cancellous bone on speed of ultrasonic fast waves in the bovine femur," *IEEE Trans. Ultrason. Ferroelectr. Freq. Control*, **55**, 1480–1487 (2008).

[8] M. A. Biot, "Generalized theory of acoustic wave propagation in porous dissipative media," *J. Acoust. Soc. Am.*, **34**, 1254–1264 (1962).
[9] K. A. Wear, "A stratified model to predict dispersion in trabecular bone," *IEEE Trans. Ultrason. Ferroelectr. Freq. Control*, **48**, 1079–1083 (2001).
[10] A. Hosokawa, "Simulation of ultrasound propagation through bovine cancellous bone using elastic and Biot's finite-difference time-domain methods," *J. Acoust. Soc. Am.*, **118**, 1782–1789 (2005).
[11] T. J. Haire and C. M. Langton, "Biot theory: A review of its application to ultrasound propagation through cancellous bone," *Bone*, **24**, 291–295 (1999).
[12] S. Chaffai, F. Padilla, G. Berger and P. Laugier, "In vitro measurement of the frequency-dependent attenuation in cancellous bone between 0.2 and 2 MHz," *J. Acoust. Soc. Am.*, **108**, 1281–1289 (2000).
[13] J. J. Kaufman, G. Luo and R. S. Siffert, "Ultrasound simulation in bone," *IEEE Trans. Ultrason. Ferroelectr. Freq. Control*, **55**, 1205–1218 (2008).
[14] E. Bossy, F. Padilla, F. Peyrin and P. Laugier, "Three-dimensional simulation of ultrasound propagation through trabecular bone structures measured by synchrotron microtomography," *Phys. Med. Biol.*, **50**, 5545–5556 (2005).
[15] F. Padilla, E. Bossy, G. Haïat, F. Jenson and P. Laugier, "Numerical simulation of ultrasound transmission in cancellous bone," *2005 IEEE Ultrason. Symp.*, Vol. 4, pp. 2022–2025 (2005).
[16] G. Haïat, F. Padilla, F. Peyrin and P. Laugier, "Variation of ultrasonic parameters with microstructure and material properties of trabecular bone: A 3D model simulation," *J. Bone Miner. Res.*, **22**, 665–674 (2007).
[17] Y. Nagatani, H. Imaizumi, T. Fukuda, M. Matsukawa, Y. Watanabe and T. Otani, "Applicability of finite-difference time-domain method to simulation of wave propagation in cancellous bone," *Jpn. J. Appl. Phys.*, **45**(9A), 7186–7190 (2006).
[18] Y. Nagatani, K. Mizuno, T. Saeki, M. Matsukawa, T. Sakaguchi and H. Hosoi, "Numerical and experimental study on the wave attenuation in bone — FDTD simulation of ultrasound propagation in cancellous bone —," *Ultrasonics*, **48**, 607–612 (2008).
[19] F. Padilla, E. Bossy and P. Laugier, "Simulation of ultrasound propagation through three-dimensional trabecular bone structures: Comparison with experimental data," *Jpn. J. Appl. Phys.*, **45**(8A), 6496–6500 (2006).
[20] F. Jenson, F. Padilla, V. Bousson, C. Bergot, J.-D. Laredo and P. Laugier, "In vitro ultrasonic characterization of human cancellous femoral bone using transmission and backscatter measurements: Relationships to bone mineral density," *J. Acoust. Soc. Am.*, **119**, 654–663 (2006).
[21] T. Otani, "Quantitative estimation of bone density and bone quality using acoustic parameters of cancellous bone for fast and slow waves," *Jpn. J. Appl. Phys.*, **44**(6B), 4578–4582 (2005).
[22] K. S. Yee, "Numerical solution of initial boundary value problems involving Maxwell's equations in isotropic media," *IEEE Trans. Antenna Propag.*, **AP-14**, 302–307 (1966).
[23] E. F. Toro, J. F. Clarke and E. F. Toro, *Numerical Methods for Wave Propagation* (Kluwer Academic Pub., Norwell, Mass., 1998).
[24] R. L. Higdon, "Absorbing boundary conditions for difference approximations to the multi-dimensional wave equation," *Math. Comput.*, **47**, 437–459 (1986).
[25] M. Sasso, G. Haïat, Y. Yamato, S. Naili and M. Matsukawa, "Frequency dependence of ultrasonic attenuation in bovine cortical bone: An in vitro study," *Ultrasound Med. Biol.*, **33**, 1933–1942 (2007).
[26] M. Sasso, G. Haïat, Y. Yamato, S. Naili and M. Matsukawa, "Dependence of ultrasonic attenuation on bone mass and microstructure in bovine cortical bone," *J. Biomech.*, **41**, 347–355 (2008).
[27] Y. Yamato, H. Kataoka, M. Matsukawa, K. Yamazaki, T. Otani and A. Nagano, "Distribution of longitudinal wave velocities in bovine cortical bone in vitro," *Jpn. J. Appl. Phys.*, **44**(6B), 4622–4624 (2005).
[28] Y. Yamato, M. Matsukawa, T. Otani, K. Yamazaki and A. Nagano, "Destribution of longitudinal wave properties in bovine cortical bone in vitro," *Ultrasonics*, **44**, e233–e237 (2006).
[29] Y. Yamato, M. Matsukawa, T. Yanagitani, K. Yamazaki, H. Mizukawa and A. Nagano, "Correlation between hydroxyapatite crystallite orientation and ultrasonic wave velocities in bovine cortical bone," *Calcif. Tissue Int.*, **82**, 162–169 (2008).
[30] M. Sakamoto, M. Kawabe, M. Matsukawa, N. Koizumi and N. Ohtori, "Measurement of wave velocity in bovine bone tissue by micro-Brillouin scattering," *Jpn. J. Appl. Phys.*, **47**, 4205–4208 (2008).
[31] A. W. Nolle and P. W. Sieck, "Longitudinal and transverse ultrasonic waves in a synthetic rubber," *J. Appl. Phys.*, **23**, 888–894 (1952).
[32] Y. Tanikaga, T. Sakaguchi and Y. Watanabe, "A study on analysis of intracranial acoustic wave propagation by the finite difference time domain method," *Proc. Forum Acusticum*, Sevilla (2002).
[33] Y. Nagatani, H. Imaizumi, T. Fukuda, M. Matsukawa, Y. Watanabe and T. Otani, "FDTD simulation on the wave propagation in the cancellous bone," *8e Congres Francaise d'Acoustique - Proc.*, pp. 681–684 (2006).

Yoshiki Nagatani received B.E., M.E., and Ph.D. degrees in Engineering from Doshisha University in 2001, 2003, and 2006, respectively. He became a research fellow at the Department of Otorhinolaryngology–Head and Neck Surgery, Nara Medical University in 2006. He is currently a lecturer of the Department of Electric Engineering in Kobe City College of Technology.

Katsunori Mizuno received B.E. and M.E. degrees in Engineering from Doshisha University in 2004 and 2006, respectively. He currently works for Panasonic corporation.

Takashi Saeki received B.E. in Engineering from Doshisha University in 2007. He is a candidate of M.E. degree in Engineering at Doshisha University. He founded a venture company of information network technology and currently works for the company as a CEO.

Mami Matsukawa joined AIST (National Institute of Advanced Industrial Science and Technology) MITI (Ministry of International Trade and Industry). She received the Dr.Eng. degree from Doshisha University in 1993. Currently, she is a professor at the Faculty of Life and Medical Sciences, Graduate School of Engineering, Doshisha University.

Takefumi Sakaguchi received B.E., M.E., and Ph.D. degrees in Engineering from Doshisha University in 1997, 1999, and 2002, respectively. He is an Assistant Professor at the Department of Otorhinolaryngology-Head and Neck Surgery, Nara Medical University since 2002.

Hiroshi Hosoi graduated from Nara Medical University in 1975 and received Dr. of Medical Science degree from Kinki University in 1985. He worked for Kinki University as a research associate and associate professor. He is currently a chairman and professor in the Department of Otorhinolaryngology-Head and Neck Surgery, Nara Medical University since 1999.

Acta Oto-Laryngologica, 2009; 129(Suppl 562): 28–33

informa
healthcare

ORIGINAL ARTICLE

N1m amplitude growth function for bone-conducted ultrasound

TADASHI NISHIMURA[1], SEIJI NAKAGAWA[2], AKINORI YAMASHITA[1], TAKEFUMI SAKAGUCHI[1] & HIROSHI HOSOI[1]

[1]*Department of Otorhinolaryngology, Nara Medical University, Kashihara and* [2]*Life Electronics Laboratory, National Institute of Advanced Industrial Science and Technology (AIST), Ikeda, Japan*

Abstract

Conclusion: N1m growth indicates the differences in central auditory processing between bone-conducted ultrasound and air-conducted audible sound. *Objectives:* Bone conduction enables ultrasound to be heard by the human ear. Despite many studies, the perceptual mechanism of bone-conducted ultrasound has not yet been clarified completely. Therefore, this study investigated the ultrasonic perception of humans, especially as regards the effects of stimulus intensity or loudness. *Subjects and methods:* The effect of the stimulus level on N1m amplitude was measured over the psycho-acoustical dynamic range. *Results:* The dynamic range for 30 kHz bone-conducted ultrasound (18.2 ± 3.3 dB) was found to be significantly narrower than that for 1 kHz air-conducted sound (85.9 ± 11.9 dB). As the stimulus level increased, the N1m amplitude in response to bone-conducted ultrasound grew faster than that to air-conducted sound. Although the growth of the N1m amplitude for air-conducted sound saturated below the uncomfortable loudness level (UCL), that for bone-conducted ultrasound continued to grow above the UCL.

Keywords: *Ultrasonic perception, uncomfortable loudness level, dynamic range, magnetoencephalography*

Introduction

In general, the upper frequency limit of human hearing is approximately 20 kHz, and sounds above this frequency are called ultrasound. However, if ultrasound is delivered by bone conduction, ultrasound up to at least 100 kHz can be heard [1,2]. Although several hypotheses about this ultrasonic perception have been suggested [2], ultrasonic perception has not yet been clarified. According to the previous reports, while the cochlea may possibly be the peripheral receptor of ultrasonic perception [2,3], bone-conducted ultrasound is difficult to mask with air-conducted audible sounds [2,3], and some profoundly deaf individuals are able to hear bone-conducted ultrasound [3–5]. These results indicate that the perceptual mechanism of bone-conducted ultrasound differs from that of air-conducted audible sound in several respects.

Several clinical applications of ultrasonic perception have been suggested, such as the treatment of tinnitus [6,7] and the diagnosis of sudden deafness, Meniere's disease [8], and noise-induced hearing loss [2]. The most interesting application may be to hearing aid technology. Lenhardt et al. [4] reported that bone-conducted ultrasonic hearing supported frequency discrimination and speech detection not only in subjects with normal hearing, but also in the elderly hearing-impaired and the profoundly deaf. They suggested that bone-conducted ultrasonic hearing might be used as an alternate communication channel in the rehabilitation of hearing disorders. Recently, Hosoi et al. observed the brain region activated by bone-conducted ultrasound using magnetoencephalography (MEG) [5]. They reported that the auditory cortex was activated by bone-conducted ultrasound, and that ultrasound modulated by different speech sounds can be discriminated in the auditory cortex. These results support the concept that bone-conducted ultrasound is recognized as an auditory sense in the

Correspondence: Tadashi Nishimura MD PhD, Department of Otolaryngology, Nara Medical University, 840 Shijo-cho, Kashihara, Nara 634-8522, Japan. Tel: +81 744 22 3051. Fax: +81 744 24 6844. E-mail: t-nishim@naramed-u.ac.jp

(Received 19 March 2009; accepted 23 March 2009)

ISSN 0001-6489 print/ISSN 1651-2251 online
DOI: 10.1080/00016480902915707

brain, and that it is possible to create an ultrasonic hearing aid for the profoundly hearing impaired to be used instead of a cochlear implant.

Despite the great potential of ultrasonic perception, it is difficult to use it clinically due to the poor establishment of its perceptual mechanism. Although the auditory cortex is involved in ultrasonic perception, how bone-conducted ultrasound is processed in the central auditory system is not well known. If the effects of ultrasonic stimuli were determined in detail, the results would contribute to the clarification of ultrasonic perception. In this study, the dynamic range and the growth of N1m amplitude over the dynamic range were measured, to determine the effect of the stimulus level on bone-conducted ultrasound processing in the central auditory system.

Subjects and methods

Nine volunteers with normal hearing took part in this study (two females and seven males; aged 24–30 years; all right-handed). The dynamic range for bone-conducted ultrasound was first compared with that for air-conducted audible sound. Second, the auditory cortical activations evoked by both sounds were compared using a neuromagnetometer (Neuromag-122, Neuromag Ltd, Helsinki, Finland). In both experiments, the ultrasound frequency was set at 30 kHz and that of the air-conducted sound at 1 kHz. The ultrasound was delivered to the mastoid via a newly devised ceramic vibrator which produces no magnetic noise. The air-conducted sound was delivered to the ear by a headphone and an earphone (E-A-R TONE 3A, Cabot Safety Co., Indianapolis, IN, USA) for the psycho-acoustical measurements and MEG study, respectively. Both sounds were generated by a function generator (WF1946, NF Electronic Instruments Co., Yokohama, Japan). The ultrasound signal was increased by a high-speed power amplifier (HSA4011, NF Electronic Instruments Co.). The signal intensities were controlled logarithmically by an attenuator (PA5, Tucker-Davis Technologies, Gainesville, USA) in order to use a decibel scale.

Measurement of the psycho-acoustical dynamic range

The experiment was performed in a soundproof room. The thresholds for both sounds were first measured using an ascending technique. The stimulus duration was set at 300 ms, including rise and fall ramps of 50 ms. The stimulus rate was set at 2 Hz. The incremental steps of the bone-conducted ultrasound and air-conducted sound were set at 1 and 5 dB, respectively. The threshold was determined when the subject responded to the signal at the same threshold in at least three ascending series. After measuring the threshold, the uncomfortable loudness level (UCL) was measured twice. The second UCL was used to estimate the dynamic range for each subject. The dynamic range was calculated by subtracting the threshold from the UCL.

MEG study

The auditory cortical activations evoked by the bone-conducted ultrasound and air-conducted sound were recorded using the neuromagnetometer in a magnetically shielded room. The magnetic responses were compared using the N1m peak amplitude measurements. Taking the results of the dynamic range measurement into consideration, the intensity level of the bone-conducted ultrasound was set at 5, 10, 15, and 20 dB SL (sensation level, based on each subject's threshold measured before the experiment) and that of the air-conducted sound was set at 45, 65, 85, and 105 dB HL. The bone-conducted ultrasound and air-conducted sounds were delivered to the left mastoid and left ear, respectively. The stimulus durations were 30 ms including rise and fall ramps of 10 ms. The inter-stimulus interval was set at 2.0 ± 0.1 s. The subjects watched a self-chosen silent movie and were instructed to pay no attention to the acoustic stimuli during the experiment. The magnetic data were sampled at 0.4 kHz after bandpass filtering between 0.03 and 100 Hz, and then averaged more than 100 times. Any responses coinciding with magnetic signals exceeding 3000 fT/cm were rejected from further analysis. The averaged responses were digitally bandpass filtered between 0.1 and 30 Hz. The analysis epoch was 0.6 s, beginning 0.1 s before the stimulus onset. The average 0.1 s pre-stimulus period served as the baseline. The neuromagnetometer has two pick-up coils in each position, which measure two tangential derivatives, $\delta Bz/\delta x$ and $\delta Bz/\delta y$, of the field component Bz. We determined:

$$B' = \sqrt{(\delta \mathrm{Bz}/\delta x)^2 + (\delta \mathrm{Bz}/\delta y)^2}$$

for each sensorposition.

For the amplitude of each subject, we employed a N1m peak amplitude with the maximum amplitude placed over the right temporal area. According to the previous report [9], N1m was determined as follows: the latency of the peak ranges between 70 and 150 ms, and the direction of the equivalent current dipole (ECD) points toward the neck. The N1m amplitudes evoked by the bone-conducted ultrasound and air-conducted sound were normalized to the respective maximum values.

Results

Psycho-acoustical measurement

The threshold and UCL for the 1 kHz air-conducted sound were 3.8 ± 7.4 and 89.7 ± 10.5 dB HL, respectively. The dynamic ranges for the bone-conducted ultrasound and air-conducted sound were 18.2 ± 3.3 and 85.9 ± 11.9 Db, respectively (Figure 1). The dynamic range for the bone-conducted ultrasound was significantly narrower than that for the air-conducted sound ($p < 0.01$).

MEG study

Figure 2 shows the magnetic response to the 20 dB SL bone-conducted ultrasound stimulus in a subject. The responses were observed over the right and left auditory cortex, and the N1m deflections over the right auditory cortex (contralateral to the stimulation side) were larger than those over the left. Figure 2 also shows the waveform of the N1m amplitude at the sensor where the maximum N1m amplitude was measured, and the isocontour map at the peak amplitude latency. The ECD was estimated over the right auditory cortex. Figure 3 shows the N1m amplitude at the sensor where the maximum N1m amplitude was measured in another subject. In this subject, the N1m in response to bone-conducted ultrasound showed a broad deflection in comparison with that to the air-conducted sound. The higher the intensity, the larger the mean N1m amplitude for both stimuli. For the 20 dB SL bone-conducted ultrasound stimulus, an artifact deflection made by the vibrator was observed. A similar artifact deflection was observed in some subjects at high stimulus levels. Figure 4 shows the mean N1m amplitude as a function of stimulus level. Basically, the higher the intensity, the larger the mean N1m amplitude for both stimuli. As the intensity increased, the growth of the N1m amplitude decreased. While the growth of the N1m amplitude for the air-conducted sound was saturated at approximately 85 dB HL, the growth of the N1m amplitude for the bone-conducted ultrasound increased beyond the UCL. Finally, the N1m amplitude in response to the bone-conducted ultrasound was approximately half as large as that to the air-conducted sound in almost all subjects.

Figure 5 shows the latency of the N1m amplitude peak. The higher the stimulus level, the shorter the latency of the amplitude peak for both stimuli. However, no significant difference was found among the stimulus levels.

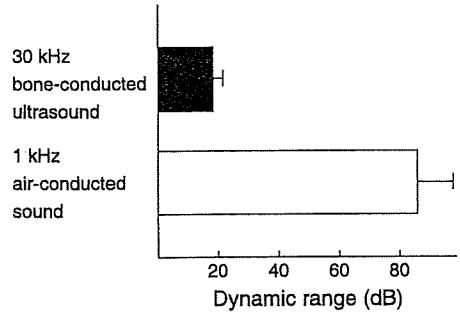

Figure 1. Dynamic ranges for 30 kHz bone-conducted ultrasound (shaded bar) and 1 kHz air-conducted sound (open bar). The bars indicate standard deviation.

Discussion

The results show that the dynamic range for the bone-conducted ultrasound is significantly narrower than that for the air-conducted sound. A similarly narrow dynamic range was also observed in the cochlear hearing-impaired [10] and those with cochlear implants [11]. Since the wide dynamic range for air-conducted sounds depends upon the outer hair cell (OHC) function [10], the lack of OHC function results in a narrow dynamic range. Therefore, the narrow dynamic range for bone-conducted ultrasound suggests the possibility that the perceptual mechanism of bone-conducted ultrasound is independent of the OHC function. In animal models, Ohyama et al. [12] investigated ultrasonic perception by electrocochleography using kanamycin-poisoned guinea pigs with damaged OHC function. While a reduction in auditory nerve action potential (AP) responses evoked by clicks was observed in the kanamycin-poisoned animals, no difference was observed in the AP responses evoked by bone-conducted ultrasound between normal and kanamycin-poisoned guinea pigs. They concluded that ultrasonic perception was mediated by inner hair cell function, independent of the OHC function. Thus, it appears that the perceptual mechanism of bone-conducted ultrasound is independent of the OHC function in man, and the narrower dynamic range of ultrasonic perception may depend on a peripheral perceptual mechanism. However, Ohyama's hypothesis originated from animal models whose ultrasonic range is different to humans. It is, therefore, necessary to address whether ultrasonic perception in man is identical to ultrasonic perception in animals.

In the MEG results for bone-conducted ultrasound, the N1m amplitude showed various shapes, for instance, a sharp deflection like an air-conducted sound (Figure 2) or a broad deflection (Figure 3). Since such distributed isocontour was observed, particularly at low stimulus levels, it was difficult to identify a reliable ECD with a single dipole model. For the reliability of intensity estimation, this study

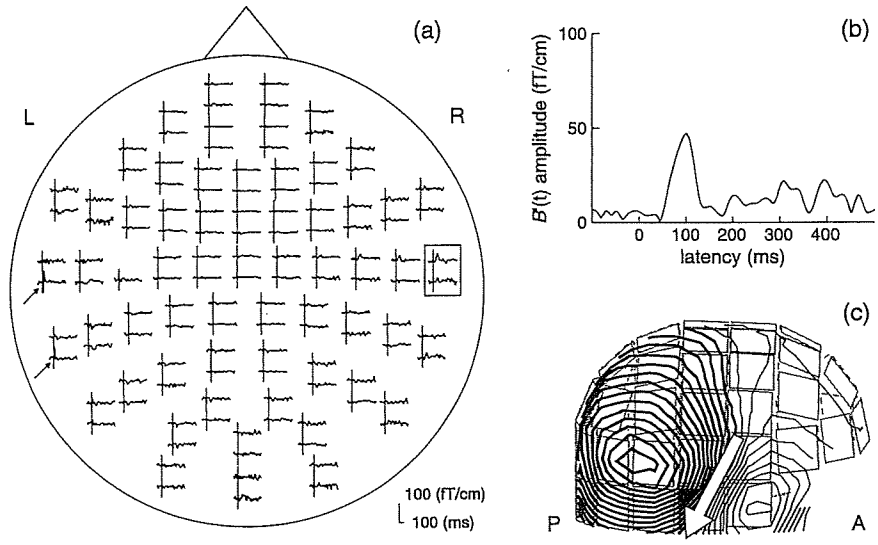

Figure 2. (a) Waveform of brain magnetic field in response to 20 dB SL bone-conducted ultrasound stimulus from 122 channels except 1 bad channel. The selected sensor indicates the maximum N1m amplitude measured. The vertical bars indicate the stimulus onset. Arrows indicate an artifact. (b) Waveform of the amplitude of the brain magnetic field (B') at the selected sensor. (c) The isocontour map (10 fT steps) at the N1m amplitude peak. The thick and thin lines indicate outgoing and incoming fields, respectively. The arrow indicates the approximate position of the equivalent current dipole.

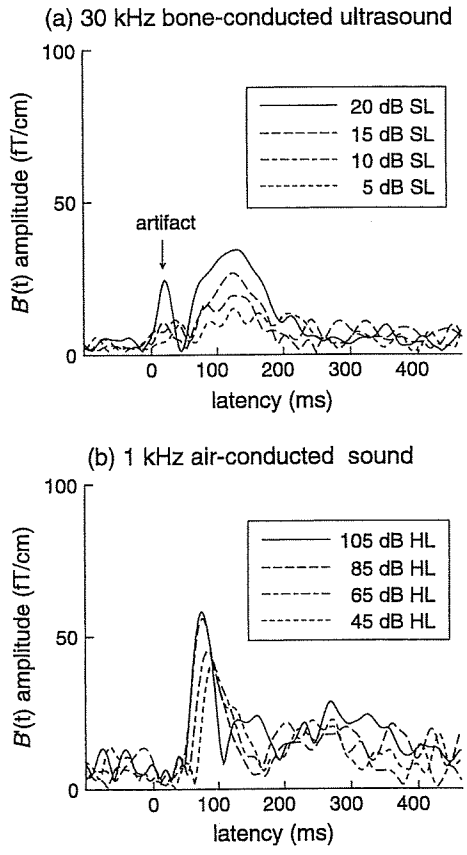

Figure 3. Waveforms of the amplitude of the brain magnetic field (B') in response to 30 kHz bone-conducted ultrasound (a) and 1 kHz air-conducted sound (b) at each intensity of a single subject. These waveforms were measured in the channel that showed the maximum amplitude over the right auditory cortex.

investigated the effects of stimulus level with maximum N1m amplitude.

In regard to N1m amplitude for the air-conducted sound, as the stimulus level increased, the growth of the N1m amplitude decreased, and was saturated below the UCL. Previous studies found the slow N1m amplitude growth at moderate stimulus levels [13]. Furthermore, at high stimulus levels, not only saturation of the growth [14] but also a decay of N1 amplitude was observed in the previous studies [15]. Thus, the growth of the N1m amplitude in Figure 4 is consistent with the previous studies. On the other hand, for bone-conducted ultrasound, the growth of the N1m amplitude decreased as the stimulus level increased, but was not saturated below the UCL. Therefore, these results revealed differences in N1m amplitude growth between the bone-conducted ultrasound and air-conducted sound.

To address the differences in central auditory processing of both sounds, the neural activity in the peripheral auditory pathways may be considered as follows. In previous reports, the growth of AP responses for air-conducted sound showed a typical two-segment curve (L-part and H-part) [16]. On the other hand, despite the results from animal models, the growth of AP responses for bone-conducted ultrasound showed a simple monotone curve, lacking the L-part [12]. Thus, the peripheral activity is assumed to be like that shown in Figure 6. While the N1m amplitude in response to air-conducted sound is less affected by change in the peripheral activity, the growth of the N1m amplitude for bone-conducted ultrasound was similar to that in Figure 6,

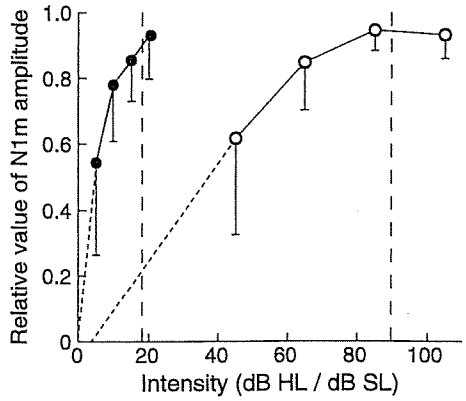

Figure 4. Mean N1m amplitude as a function of stimulus intensity for 30 kHz bone-conducted ultrasound (solid circles connected by a solid line) and 1 kHz air-conducted sound (open circles connected by a solid line). The N1m amplitudes for the bone-conducted ultrasound and air-conducted sound were normalized to the respective maximum values in each subject. The vertical lines indicate the uncomfortable loudness level (UCL) for 30 kHz bone-conducted ultrasound (left vertical dashed line) and 1 kHz air-conducted sound (right vertical dashed line). The bars indicate standard deviation.

implying that the N1m amplitude in response to bone-conducted ultrasound largely depends on peripheral activity.

Judging from these growth curves (Figure 4 and 6), recruitment may account for the current results. For the hearing-impaired subjects, the dynamic range is smaller than that in the normal-hearing subjects [10]. The AP growth shows a steep curve similar to that in response to bone-conducted ultrasound in Figure 6

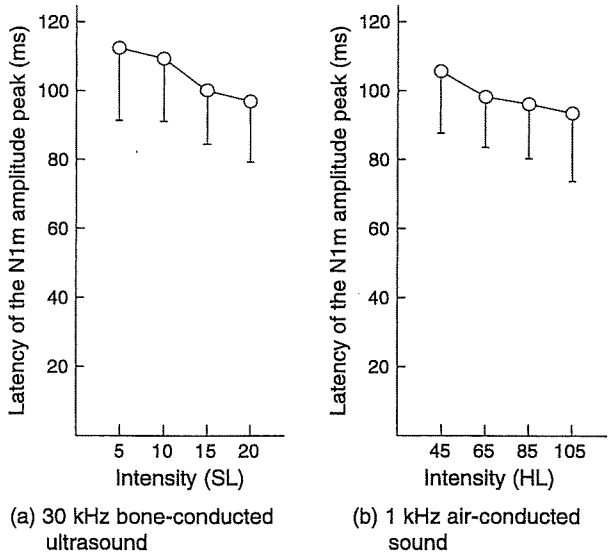

Figure 5. Mean latency of the N1m amplitude peak as a function of stimulus intensity for 30 kHz bone-conducted ultrasound (a) and 1 kHz air-conducted sound (b). The bars indicate standard deviation.

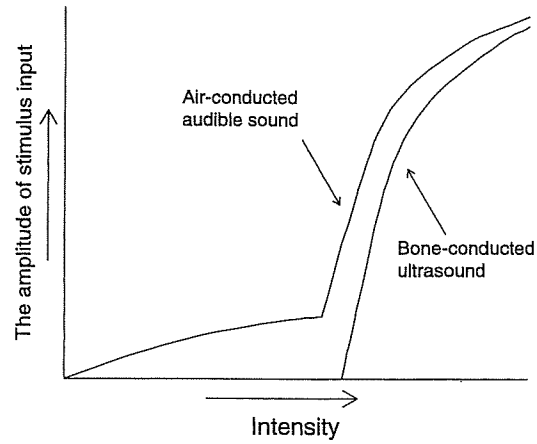

Figure 6. A schematic illustration of the activity in the peripheral auditory pathways as a function of the stimulus level for bone-conducted ultrasound and air-conducted sound. For air-conducted sound, the curve consists of two segments termed the L-part and the H-part. On the other hand, for bone-conducted ultrasound, the curve shows a simple monotonic growth, lacking the L-part.

[17], and the N1 amplitude grew faster than that in the normal-hearing subjects [15]. These characteristics correspond to those observed for bone-conducted ultrasound in our results. Therefore, the faster growth of N1m amplitude for bone-conducted ultrasound may depend on the same mechanism as recruitment in the hearing impaired. Since the threshold of hearing increases rapidly above a high frequency even in normal hearing, all subjects may be considered to be hearing impaired at high-frequency tones. Thus, our results suggest that bone-conducted ultrasound is perceived by the human auditory system in the same manner as the hearing impaired perceives air-conducted sound.

In this study, the vibrator used emitted no air-conducted audible sound, and no response was evoked if the vibrator was kept away from the body. In terms of the perceptual mechanism of bone-conducted ultrasound, several reports have indicated the possibility of sub-harmonic audible sound generation in the transmission path [2,18]. Since it is difficult to estimate sound field accurately in the cochlea, it has not yet been concluded whether ultrasonic perception is provided by ultrasound itself or by sub-harmonic sounds. However, even if sub-harmonic sounds are generated, ultrasound cannot be perceived by air conduction, implying that the perceptual mechanism of bone-conducted ultrasound may differ from that of air-conducted audible sound in several respects.

Conclusion

In this study, the effect of the stimulus level on bone-conducted ultrasound was measured using a

psycho-acoustical method and MEG. The psycho-acoustical dynamic range for 30 kHz bone-conducted ultrasound was found to be significantly narrower than that for 1 kHz air-conducted sound. If bone-conducted ultrasound is used in clinical applications, its output level should be carefully set to avoid noise-induced hearing loss. In regard to central auditory processing, the effect of the stimulus level on the growth of N1m amplitude for the bone-conducted ultrasound was larger than that for air-conducted sound. Although the growth of the N1m amplitude for air-conducted sound was saturated below the UCL, the N1m amplitude for bone-conducted ultrasound continued to grow above the UCL. Considering the activity in the peripheral auditory pathways, it appears that the N1m amplitude in response to bone-conducted ultrasound is largely affected by the stimulus level, similar to the growth of the N1m amplitude in the hearing impaired. These results show the differences in the central auditory processing between bone-conducted ultrasound and air-conducted sound.

Declaration of interest: The authors report no conflicts of interest. The authors alone are responsible for the content and writing of the paper.

References

[1] Pumphrey R. Upper limit of frequency for human hearing. Nature 1950;166:571.

[2] Dieroff HG, Ertel H. Some thoughts on the perception of ultrasonics by man. Arch Otorhinolaryngol 1975;209: 277–90.

[3] Bellucci R, Schneider D. Some observations on ultrasonic perception in man. Ann Otol Rhinol Laryngol 1962;71: 719–26.

[4] Lenhardt ML, Skellett R, Wang P, Clarke AM. Human ultrasonic speech perception. Science 1991;253:82–5.

[5] Hosoi H, Imaizumi S, Sakaguchi T, Tonoike M, Murata K. Activation of the auditory cortex by ultrasound. Lancet 1998;351:496–7.

[6] Carrick DG, Davies WM, Fielder CP, Bihari J. Low-powered ultrasound in the treatment of tinnitus: a pilot study. Br J Audiol 1986;20:153–5.

[7] Rendell RJ, Carrick DG, Fielder CP, Callaghan DE, Thomas KJ. Low-powered ultrasound in the inhibition of tinnitus. Br J Audiol 1987;21:289–93.

[8] Abramovich SJ. Auditory perception of ultrasound in patients with sensorineural and conductive hearing loss. J Laryngol Otol 1978;92:861–7.

[9] Näätänen R, Picton T. The N1 wave of the human electric and magnetic response to sound: a review and analysis of the component structure. Psychophysiology 1987;24:375–425.

[10] Davis H. An active process in cochlear mechanics. Hear Res 1983;9:79–90.

[11] Shannon RV. Multichannel electrical stimulation of the auditory nerve in man. I. Basic psychophysics. Hear Res 1983;11:157–89.

[12] Ohyama K, Kusakari J, Kawamoto K. Sound perception in the ultrasonic region. Acta Otolaryngol Suppl 1987;435: 73–7.

[13] Pantev C, Hoke M, Lehnertz K, Lütkenhöner B. Neuromagnetic evidence of an amplitopic organization of the human auditory cortex. Electroencephalogr Clin Neurophysiol 1989;72:225–31.

[14] Reite M, Zimmerman JT, Edrich J, Zimmerman JE. Auditory evoked magnetic fields: response amplitude vs. stimulus intensity. Electroencephalogr Clin Neurophysiol 1982;54:147–52.

[15] Uziel A, Seneclause S. Electrophysiological investigation of auditory recruitment by averaged electroencephalographic-evoked response. Audiology 1978;17:141–51.

[16] Yoshie N. Auditory nerve action potential responses to clicks in man. Laryngoscope 1968;78:198–215.

[17] Dallos P, Harris D. Properties of auditory nerve responses in absence of outer hair cells. J Neurophysiol 1978;41:365–83.

[18] Haeff AV, Knox C. Perception of ultrasound. Science 1963; 139:590–2.

Acta Oto-Laryngologica, 2009; 129(Suppl 562): 34–39

informa
healthcare

ORIGINAL ARTICLE

Comparison between bone-conducted ultrasound and audible sound in speech recognition

AKINORI YAMASHITA, TADASHI NISHIMURA, YOSHIKI NAGATANI, TADAO OKAYASU, TOSHIZO KOIZUMI, TAKEFUMI SAKAGUCHI & HIROSHI HOSOI

Department of Otolaryngology, Nara Medical University, Kashihara Nara, Japan

Abstract

Conclusion: This study showed that it is possible to transmit language information using bone-conducted ultrasound (BCU) in normal-hearing subjects. Our results suggest the possibility of a difference in speech recognition between BCU and air-conducted audible sound (ACAS). *Objective:* Ultrasound was audible when delivered by bone conduction. Some profoundly deaf subjects as well as normal-hearing subjects can discriminate BCU whose amplitude is modulated by different speech sounds. These findings suggest the usefulness of developing a bone-conducted ultrasonic hearing aid (BCUHA). However, the characteristics of BCU are still poorly understood. The aim of the present study was to compare BCU and ACAS in terms of their associated speech perception tendency and to investigate the different perceptual characteristics of BCU and ACAS. *Subjects and methods:* Speech discrimination tests using both BCU and ACAS were performed with normal-hearing subjects. BCU and ACAS were compared for intelligibility and hearing confusion. *Results:* With BCU, the maximum percentage correct totaled about 75%. Our comparison of the hearing confusion with ACAS and BCU according to the individual syllabic nuclear group showed a clear difference in the incorrect rates. In addition, the stimulus nuclear groups were often perceived in other nuclear groups in BCU.

Keywords: *Ultrasonic speech perception, List 67-S, amplitude modulation, bone-conducted ultrasonic hearing aid, intelligibility, monosyllable, hearing confusion*

Introduction

It is generally thought that humans can perceive sound by air conduction in the frequency range of approximately 16 Hz to 24 kHz [1]. However, several studies have reported that ultrasound in a frequency range up to at least 120 kHz can be perceived through bone conduction [2–4]. Since this phenomenon was first reported [2], several hypotheses about this ultrasonic perception have been suggested. One report postulates that a certain biomechanical system demodulates the ultrasound into low-frequency audible sound [5], while others hypothesize a contribution by cochlear hair cells [3,4,6–8] or vestibular hair cells [9,10]. Despite many later studies, however, no consensus has emerged regarding the perception mechanism of bone-conducted ultrasound (BCU). In terms of the perceptual characteristics of BCU, several differences between BCU and air-conducted audible sound (ACAS) have been reported. For instance, the subjective pitch elicited by BCU is similar to the pitch of air-conducted sound in the 8–16 kHz range [3,4,6]. BCU can mask perception of ACAS in the 10–14 kHz range, and this masking phenomenon is independent of ultrasonic frequency [8]. The dynamic range of BCU is narrower than that of ACAS [8]. The most interesting characteristic of ultrasonic perception is that some profoundly hearing-impaired individuals can perceive BCU. Lenhardt et al. reported that frequency discrimination is possible in those who perceive BCU [10]. They also reported that the speech signals that modulate the carrier wave of BCU can be detected not only by normal-hearing subjects but also by elderly hearing-impaired and profoundly deaf subjects. These findings support the idea of an ultrasonic hearing aid system for profoundly deaf subjects. Recently,

Correspondence: Akinori Yamashita, Department of Otolaryngology, Nara Medical University, 840 Shijo-cho, Kashihara Nara 634-8522, Japan. Tel: +81 744 29 8887. Fax: +81 744 24 6844. E-mail: akinori@naramed-u.ac.jp

(Received 24 March 2009; accepted 26 March 2009)

ISSN 0001-6489 print/ISSN 1651-2251 online
DOI: 10.1080/00016480902926449

magnetoencephalography (MEG) and positron emission tomography (PET) studies have objectively demonstrated that the auditory cortex of some profoundly deaf subjects can discriminate ultrasounds whose amplitudes are modulated by different speech sounds [11–13]. These studies also support the potential for the development of a bone-conducted ultrasonic hearing aid (BCUHA) that could be used by elderly hearing-impaired and profoundly deaf subjects. Using the findings of these reports, Nakagawa et al. developed a BCUHA and investigated its usefulness for profoundly deaf subjects [14]. In that study, all normal-hearing subjects could sense BCU modulated by speech signals and 50% of them could clearly detect Japanese words; however, in the case of deaf subjects, only 40% could sense BCU and 20% could detect Japanese words. Okamoto et al. investigated the intelligibility of bone-conducted ultrasonic speech in normal-hearing subjects using a Japanese monosyllable list compiled in a commercially available database (NTT Advanced Technology Corporation) [15]. They reported that the highest average score from monosyllable intelligibility tests with BCU was about 60%. The monosyllable list is usually used for speech discrimination tests in Japan; however, the list is not often used in the speech discrimination test for evaluation of the hearing impaired in Japan. The list most commonly used in the speech discrimination test is List 67-S authorized by the Japan Audiological Society. List 67-S comprises 20 monosyllables used frequently in daily conversation. This list is also used for adaptation to hearing aids, hearing aid evaluations, and adaptation to cochlear implants. In BCU, therefore, the use of List 67-S in speech discrimination tests is very important for the development of BCU through comparison with the enormous quantity of data available.

In this study, we used List 67-S to measure the intelligibility of Japanese monosyllables in BCU and ACAS among normal-hearing subjects. We compared BCU and ACAS in terms of the tendency to perceive speech and investigated the difference between BCU from ACAS in terms of perceptual characteristics.

Subjects and methods

Subjects

Thirteen adults (seven males and six females) took part in the experiment. All were native Japanese speakers. All subjects had hearing within 20 dB HL at all frequencies from 125 to 8000 Hz as measured by conventional pure tone audiometry (AA-78; Rion, Tokyo Japan). All subjects encountered BCU for the first time in this experiment. The subjects' ages ranged from 21 to 29 years. Informed consent was obtained from each subject after the nature of this study was explained.

Stimuli

Speech discrimination tests were performed with both BCU and ACAS using List 67-S, which comprises 20 monosyllables (/a/, /ta/, /ha/, /ba/, /ga/, /wa/, /ki/, /shi/, /ji/, /ni/, /ri/, /u/, /ku/, /su/, /te/, /ne/, /o/, /mo/, /to/, /yo/). In the experiment with BCU, a 30 kHz sinusoidal wave was used as the carrier wave because the resonance frequency of the vibrator was around 30 kHz, and this signal wave was amplitude-modulated with speech signals. For calibration, a 1 kHz sinusoidal wave for level proofreading attached to List 67-S CD was used. This wave taped at the average output level of speech signals. Modulation was set at 100% of this sinusoidal wave. The modulated signal is expressed in the following formula:

$$U(t) = (S(t) - S_{min}) \times \sin(2\pi f_c t)$$

where S(t) indicates the speech signal, S_{min} is the minimum amplitude value of S(t), and f_c indicates the 30 kHz carrier wave. Figure 1 shows an example of the waveform of a monosyllable speech signal and the ultrasonic waveforms modulated by the speech signal.

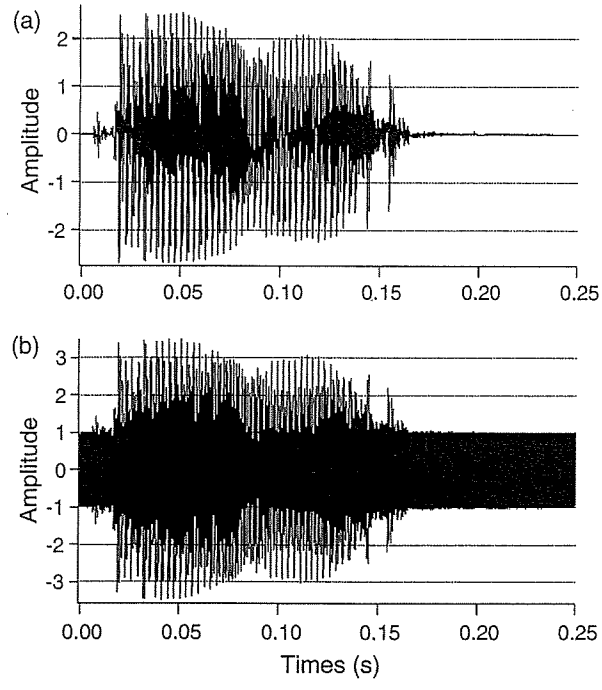

Figure 1. Waveforms of a monosyllable signal (/a/). (a) Monosyllable signal in the audible range. (b) Monosyllable signal amplitude modulated into the ultrasonic range.

Procedure

The ultrasonic stimuli were delivered to the right mastoid via a custom-made ceramic vibrator. At the beginning of the experiment, the subjects' ability to hear ultrasound by bone conduction was investigated with a 30 kHz sinusoidal wave amplitude-modulated with a 1 kHz tone burst. (Stimulus duration was set at 200 ms with rising/falling ramps of 20 ms and a stimulus rate of 2 Hz.) The tone burst was made from the sinusoidal wave at 1 kHz for level proofreading. For subjects who could hear BCU, the sensation threshold was measured and the threshold was set at 0 dB. After measurement of the thresholds, we measured the uncomfortable loudness level (UCL) and the most comfortable loudness level (MCL). The threshold of sensation, MCL, and UCL of each subject were determined by an ascending technique. Measurements were performed at least three times. If differences in threshold of measurement were within 1 dB, we employed the average. If the response was unstable, measurement was discontinued and begun again. The stimulus rate was set at 2 Hz. The step size was 0.1 dB.

After the measurement of the MCL and UCL, the speech discrimination test with BCU was performed. The carrier wave was modulated with monosyllable sounds output from the CD provided with List 67-S. This modulation was performed with a function generator (WF1946; NF Electronic Instruments Co., Yokohama, Japan). The ultrasound signals were increased with a high-speed power amplifier (HSA4011; NF Electronic Instruments Co.). The signal intensities were controlled logarithmically with an attenuator (PA5; Tucker-Davis Technologies, Gainesville, FL, USA) in order to use the decibel scale. The intensity levels of BCU were set at 0, 5, 10, and 15 dB. The monosyllable intelligibility test with BCU was performed at every signal intensity.

The monosyllable intelligibility test with ACAS was also performed. The audible sound stimuli output from an audiometer (AA-78; Rion) were delivered to the right ear though a headphone. The intensity levels of ACAS were set at 0, 10, 20, 30, and 40 dB HL. By agreement with the Japan Audiological Society, the intensity of 0 dB generated from this audiometer is prescribed at 14 dB SPL.

The inter-stimulus interval for the monosyllable intelligibility tests both in BCU and ACAS was 3.0 s. The same 20 monosyllables were used at each sound level. The stimuli were presented in random order. Each subject was instructed to record by hand during the interval what he or she had heard. All the experiments were carried out in a soundproof room.

Result

All subjects detected a pitch when the 30 kHz sinusoidal wave amplitude modulated with a 1 kHz tone burst was delivered by bone conduction. MCL was 8.6 ± 3.3 dB SL and UCL was 18.6 ± 4.6 dB SL on average.

The results of speech discrimination tests with BCU and ACAS are shown in Figure 2. In the speech discrimination test with BCU, one subject could not perceive any speech information from the stimulus signal; therefore, this subject was excluded from the statistics. In each stimulus condition, the differences in the intelligibility of the sound levels were tested for significance by one-way ANOVA. The sound level had a significant effect for both BCU and ACAS ($p < 0.01$). This significant effect was observed in all pairs of sound levels for BCU in post hoc analysis. In the speech discrimination test with ACAS, the percentage correct totaled about 100% at a sound level of 40 dB HL; however, for

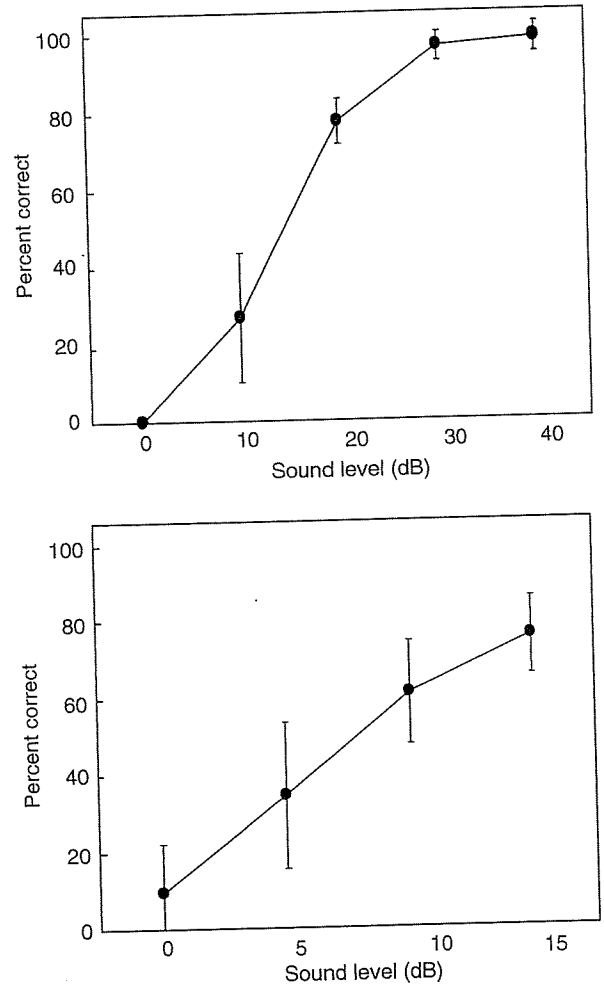

Figure 2. Averaged score of speech discrimination tests with (a) ACAS and (b) BCU. Vertical bars indicate standard deviations.

BCU, the maximum percentage correct totaled only about 75% at a sound level of 15 dB SL.

Table I shows all hearing confusion in 12 subjects with BCU at 15 dB. We compared hearing confusion at 15 dB for BCU with that at 20 dB for ACAS. The percentage correct was approximately equal in each case. Table II shows the total number of cases of hearing confusion for the individual syllabic nuclear group of /a/, /i/, /u/, /e/, and /o/. The wrong rates with the nuclei /i/ for ACAS and BCU were 28.3% and 15%, respectively. On the other hand, the wrong rate with the nuclei /e/ for ACAS was 5.0%, increasing significantly to 45.8% for BCU. Table III shows the confusion matrix for the individual syllabic nuclear groups. The numbers in the table indicate the percentages of incorrect responses in each syllabic nuclear group. Almost all stimuli for ACAS resulted in a score of 100%; for BCU, the stimulus nuclear groups of /a/ and /i/ showed hearing confusion with the same nuclear groups; however, the stimulus nuclear groups of /u/, /e/, and /o/ often showed hearing confusion with other nuclear groups.

Discussion

Measurements of MCL and UCL levels are generally required to determine the parameters to be used for hearing aid devices. In this study, the MCL for BCU was 3.3–12.7 dB SL and 8.6 dB SL among all subjects on average. Although no speech discrimination test was performed at MCL, it is predicted from the results of the sound levels at 5 and 10 dB SL that the percentage correct at MCL would be about 50%. It is generally agreed that the intensity of conversational speech should be amplified to MCL for the hearing impaired [16]. Therefore, the hearing impaired will require the hearing aid gain to be set to the intensity of MCL. If the levels of intelligibility are similar in profoundly deaf subjects who can sense BCU, we can anticipate the practical application of a BCUHA.

In the experiment, one subject could not perceive any speech information from the stimulus signal. Because the mechanisms of BCU perception are still unclear, it is difficult to specify the reason for this. One possible reason for it involves the characteristics of BCU, especially pitch. The subjective pitch elicited by ultrasonic stimulation has been found to be independent of its frequency, and it is perceived as if it were due to air-conducted stimuli of 8–16 kHz [3,4,6]. This characteristic indicates that the pitch of BCU fluctuates and that pitch change is unstable, i. e. that increase in frequency does not always lead to subjective increase in pitch. There are thus large differences between subjects in perception of BCU modulated by speech signals. Moreover, some subjects find BCU stimulation uncomfortable due to its high pitch. The subject at issue might thus not have been able to recognize speech sounds included within the ultrasound. We will examine this subject in greater detail in future work, since this may yield important findings concerning the mechanism of ultrasound perception.

Okamoto et al. [15] reported that the highest average scores from monosyllable intelligibility tests for BCU were about 60% and that the monosyllable intelligibility scores for BCU at 25 dB and 30 dB showed no significant difference. They noted that the intelligibility of BCU is not necessarily relative to the sound level. This phenomenon might arise because the subjects perceive both the speech sound

Table I. All incorrect responses from 12 subjects with BCU at 15 dB.

Stimulus		Incorrect responses						
/a/	→	/ni/						
/ta/	→	/sa/	/tsu	/a/				
/ha/	→	/ta/	/ta/	/ta/	/ta/	/hi/	/ka/	/a/
/ba/	→	/ka/	/ra/	/da/	/da/	/ta/		
/ga/	→	/da/	/do/	/de/				
/wa/	→	/ra/	/ro/	/ha/				
/ki/	→	/i/	/i/					
/shi/	→	/hi/						
/ji/	→	/chi/	/chi/					
/ni/	→	/u/	/ri/					
/ri/	→	/bi/	/ji/					
/u/	→	/a/	/i/	/i/	/i/	/ni/		
/ku/	→	/ko/						
/su/	→	/shi/	/sa/					
/te/	→	/ko/	/ko/	/me/	/to/	/ha/	/ne/	/de/
/ne/	→	/to/	/me/	/ba/	/ri/			
/o/	→	/a/	/ga/					
/mo/	→	/da/	/ri/	/no/				
/to/	→	/ko/	/ho/	/pa/	/o/			
/yo/	→	/na/						

Table II. Total number of incorrect responses for each syllabic nuclear group with both ACAS and BCU.

Vowel syllabic nuclear group	Monosyllables in List 67-S	Total	Errors with ACAS	Errors with BCU
a (6 monosyllables)	/a/, /ta/, /ha/, /ba/, /wa/, /ga/	72	20	23
i (5 monosyllables)	/ki/, /shi/, /ji/, /ni/, /ri	60	17	9
u (3 monosyllables)	/u/, /ku/, /su/	36	11	8
e (2 monosyllables)	/te/, /ne/	24	1	11
o (4 monosyllables)	/o/, /to/, /mo/, /yo/	48	6	10

and carrier signal simultaneously. On the other hand, our results show that the highest average score for the speech discrimination tests for BCU was about 75% at 15 dB SL and that the score of the speech discrimination test with BCU increased significantly in all pairs of sound levels. These results show that the intelligibility of the speech discrimination test for BCU is not saturated and that our highest score was better than their results. It is evident that the listeners perceived high tones induced by the carrier signal more strongly as the sound levels increased. However, our results did not show an influence in carrier frequency, although this may be a result of our use of a different list, speaker, degree of modulation, and threshold search method.

Safety considerations require that the stimulating intensity be set to less than UCL. Although Okamoto et al. [15] indicated that ultrasonic stimuli were delivered without discomfort, UCL was not measured strictly in their report. In our experiments, after measuring UCL – which was 15.1–33.1 dB SL and 18.6 dB SL on average – speech discrimination tests with BCU were performed at an intensity less than UCL. In our results, the highest average score was about 75% at 15 dB SL. For safety reasons and to support the development of BCUHA, it is very important that this high intelligibility be obtained at less than UCL.

Table III. Confusion matrix for the individual syllabic nuclear groups based on the results of monosyllable intelligibility tests with ACAS and BCU.

	Incorrect response group					
Stimulus group	a	i	u	e	o	No response
ACAS						
a	100					
i		100				
u			91		9	
e				100		
o			33		67	
BCU						
a	70	9	4	4	9	4
i		89	11			
u	25	63			13	
e	18	9		36	36	
o	50	10			40	

Our comparison of hearing confusion between ACAS and BCU according to individual syllabic nuclear groups showed a clear difference in the incorrect rates. In addition, the stimulus nuclear groups were often perceived in other nuclear groups in BCU stimuli, although most incorrect responses showed hearing confusion with the same nuclear group in ACAS stimuli. These facts indicate the possibility of a difference between BCU and ACAS in terms of speech recognition methods. Further study is needed to clarify the factors behind this difference because the mechanisms of BCU perception are still unclear.

Our results indicate that vowel articulation in BCU is inferior to that of ACAS. However, this result might have been influenced by the unpracticed subjects, as all subjects in this study heard BCU for the first time in this experiment. Therefore, it is assumed that intelligibility can be improved with training.

Conclusion

In this study, we compared BCU and ACAS in terms of speech perception tendencies in subjects with normal hearing. Our results suggest that it is possible to transmit language information with BCU stimulation to normal-hearing subjects. Although the highest average score from speech discrimination testing with BCU was about 75%, it may be possible to improve intelligibility through training or by improving signal processing. However, the possibility that BCU and ACAS differ in terms of the mechanism of speech recognition has also been suggested. Therefore, further investigation is important. This result cannot be applied directly to profoundly deaf subjects. The present findings provide important clues for the development of BCUHA. Improved sound processing and further study with hearing-impaired subjects are needed to develop the BCUHA for elderly hearing-impaired and profoundly deaf subjects.

Acknowledgements

This work was supported by Grant-in-Aid for Scientific Research (B) (18390462) and Grants-in-Aid for

Research on Indoor Environmental Medicine of Nara Medical University.

Declaration of interest: The authors report no conflicts of interest. The authors alone are responsible for the content and writing of the paper.

References

[1] Wagel RP. Physical data and physiology of excitation of the auditory nerve. Ann Otol Rhinol Laryngol 1932;41:740–99.
[2] Gavreau V. Audibillite de sons frequence elevee. Compt Rendu 1948;226:2053–4.
[3] Pumphrey R. Upper limit of frequency for human hearing. Nature 1950;166:571.
[4] Dieroff HG, Ertel H. Some thoughts on the perception of ultrasound by name. Arch Otorhinolaryngol 1975;209: 277–90.
[5] Dobie RA, Wiederhold ML. Ultrasonic hearing. Science 1992;255:1584–5.
[6] Deatherage BH, Jeffress LA, Blodgett HC. A note on the audibility of intense ultrasonic sound. J Acoust Soc Am 1954;26:582.
[7] Ohyama K, Kusakari J, Kawamoto K. Ultrasonic electrocochleography in guinea pig. Hear Res 1985;17:143–51.
[8] Nishimura T, Nakagawa S, Sakaguchi T, Hosoi H. Ultrasonic masker clarifies ultrasonic perception in man. Hear Res 2003;175:171–7.
[9] Bellucci RJ, Schneider DE. Some observations on ultrasonic perception in man. Ann Otol Rhinol Laryngol 1962;71: 719–26.
[10] Lenhardt ML, Skellett R, Wang P, Clarke AM. Human ultrasonic speech perception. Science 1991;253:82–5.
[11] Hosoi H, Imaizumi S, Sakaguchi T, Tonoike M, Murata K. Activation of the auditory cortex by ultrasound. Lancet 1998;351:496–7.
[12] Nakagawa S, Yamaguchi M, Tonoike M, Watanabe Y, Hosoi H, Imaizumi S. Characteristics of auditory perception of bone-conducted ultrasound in human revealed by magnetoencephalography. Neuroimage 2000;11:s746.
[13] Imaizumi S, Hosoi H, Sakaguchi T, Watanabe Y, Sadato N, Nakamura S, et al. Ultrasound activates the auditory cortex of profoundly deaf subjects. NeuroReport 2001;12:583–6.
[14] Nakagawa S, Okamoto Y, Fujisaka Y. Development of a bone-conducted ultrasonic hearing aid for the profoundly sensorineural deaf. Trans Jpn Soc Med Biol Eng 2006;44: 184–9.
[15] Okamoto Y, Nakagawa S, Fujimoto K, Tonoike M. Intelligibility of bone-conducted ultrasonic speech. Hear Res 2005; 208:107–13.
[16] Shapiro I. Prediction of most comfortable loudness levels in hearing aid evaluation. J Speech Hear Disord 1975;40: 434–8.